

Programmable mRNA therapeutics for controlled epigenomic modulation of single and multiplexed gene expression in diverse diseases

Received: 15 November 2023

Accepted: 7 March 2025

Published online: 13 March 2025

 Check for updates

Charles W. O'Donnell^{1,2}✉, Jeremiah D. Farelli^{1,2}, Houda Belaghzal^{1,2}, Justin Chen^{1,2}, Lauren Beech¹, James Sullivan¹, Chevaun Morrison-Smith¹, Stephen Siecinski¹, Adam Katz¹, Samuel Mildrum¹, Mayur Gurnani¹, Prachi Dhanania¹, Caitlyn R. Webb¹, Giuliana Castello Coatti¹, Pranjali Rumale¹, Daniel F. G. Costa¹, Marcus I. Gibson¹, Yaoyu E. Wang¹, Joseph V. Newman¹ & Thomas G. McCauley¹

Pathogenic gene dysregulation can be attributed to chromatin state change that pre-transcriptionally regulates expression. Recent breakthroughs elucidating the rules governing this DNA control layer, an epigenetic code, unlock a modality in precision medicine to target gene dysregulation across myriad diseases. Here we present a modular platform to design programmable mRNA therapeutics, Epigenomic Controllers (EC), that control gene expression through directed epigenetic change. By leveraging natural mechanisms, ECs tune expression levels of one or multiple genes with durable effect of weeks-to-months in female mice following a single dose. We design and characterize ECs to multiple target genes and identify an EC that effectively inhibits the cancer- and inflammatory-disorder-associated multi-gene cluster *CXCL1-8*. With precision targeting of NF- κ B signaling and identification of homologous murine surrogates, ECs significantly reduce neutrophil migration in vivo during acute lung inflammation in female mice. A platform approach to EC design for epigenomic modulation expands treatment frontiers for diverse gene targets, including those considered “undruggable.”

Genetic studies have proven instrumental in identifying causal gene/disease associations¹, however, these are limited in their ability to explain pathogenic dysregulation solely through DNA variation. Moreover, association studies revealed that over 90% of disease-related genetic variation affects non-coding functional DNA regions, termed cis-regulatory elements (CREs), that distally influence gene transcription but cannot be directly targeted using traditional therapeutic treatment modalities that focus on post-transcriptional

processes. Operating in a disease-dependent and cell-type-specific manner², this epigenetic regulation is mediated by processes including methylation, acetylation, phosphorylation, sumoylation, and ubiquitylation, where DNA, histones, and other regulatory machinery are chemically modified to influence transcriptional state³. Further, recent discoveries show that gene regulation is controlled in a modular, hierarchical manner through DNA compaction and chromatin looping. Most notably, highly structured, conserved processes functionally

¹Omega Therapeutics, Inc., Cambridge, MA, USA. ²These authors contributed equally: Charles W. O'Donnell, Jeremiah D. Farelli, Houda Belaghzal, Justin Chen. ✉e-mail: odonnell@omegatx.com

insulate gene transcription within spatial modules, termed Insulated Genomic Domains (IGDs), that bring regulatory elements in proximity to activate or repress transcription (Fig. 1) (e.g., through homo-dimerization of CTCF and cohesion anchoring distal DNA sites⁴). This has revealed an epigenetic etiology unrelated to DNA mutation at the root of a vast number of diseases, including cancer, autoimmune, metabolic, cardiovascular, and neurological disorders^{5,6}.

Precision epigenomic therapies, such as epigenetic-editors⁵, present a promising approach to tackle this fundamental driver of disease, with the potential to exert pre-transcriptional control through endogenous regulatory mechanisms to durably fine-tune gene expression without permanent genetic change. Moreover, epigenetic elements lie on the critical path of gene dysregulation, so directly targeting these elements offers a high likelihood for therapeutic success. This is particularly relevant where tuning expression of one or many disease genes is required, providing therapeutic benefit over modalities such as direct silencing (via, e.g., siRNA or editing⁷) or overexpression (via, e.g., AAV-delivered gene transfer⁸). In this manner, a modular, engineered, and computationally guided framework could enable the rapid development of therapeutics that target nearly any disease process, including genes and pathways formerly believed to be “undruggable.”

We have previously shown how this approach can be effectively used to target *MYC* in hepatocellular carcinoma models⁹. However, in many disease processes and pathways, simultaneous therapeutic control of multiple genes is essential to remedy acute and chronic conditions. For example, eight functionally similar chemoattractants, CXCL1-8, are found and jointly regulated within a single IGD. This gene cluster is critical in neutrophil migration, a disease process which impacts many diseases, including acute respiratory distress syndrome (ARDS), systemic and local inflammatory disorders, and several cancers^{10,11}. Driven primarily by NF- κ B signaling, these cytokines overexpress under inflammatory conditions, initiating an acute pathological cascade via CXCR1/2 receptor signaling. Moreover, because of shared function, inhibition of only a single gene can lead to a compensatory response via the expression of other genes in the locus; thus, simultaneous multi-gene control is required for effective therapeutic benefit. This may partly explain why previous anti-CXCL8 (anti-IL-8) therapeutics have not proven effective clinically¹².

We sought to build a programmable mRNA therapeutics-based platform that enables precise, controlled epigenomic modulation to ameliorate nearly any dysregulated gene or disease process. Leveraging established mRNA therapeutic technology, we take a systematic approach (Fig. 1) to (1) map gene regulatory processes to targetable genomic loci that epigenetically operate in a cell- and disease-dependent manner, (2) design and validate a library of proteins (effectors) capable of modifying epigenetic target states, (3) optimally target these effector proteins by tethering one or more to a custom-designed DNA-binding domain (DBD), and (4) construct an Epigenomic Controller (EC), an mRNA therapeutic that produces one or several effector-DBD fusion proteins. We focus here on the development of ECs as the active drug substance of any potential clinical drug product, which would be delivered using custom tissue-specific lipid nanoparticles (LNPs). ECs represent a modular evolution of drug discovery, wherein the development and optimization of EC drug substances can proceed in parallel with the development of one or many LNPs designed for discrete and specific therapeutic applications. Therefore, while LNP development remains a critical component for the clinical success of any EC, it must be married to the therapeutic area of interest and remains beyond the scope of this publication.

ECs target three types of non-coding regulatory elements: transcriptional promoters, cis-regulatory elements (cREs), and DNA loop anchors. Platform mapping efforts identify additive, synergistic, and non-linear effects between these elements, which inform tailored targeting strategies - including multi-element and multi-IGD targeting via multi-cistronic mRNA. DBDs employed include algorithmically optimized zinc finger-like proteins (ZFPs), transcription activator-like effectors (TALs), and other DBD constructs, while effectors may include, but are not limited to, DNA methyltransferases, methylcytosine dioxygenases, transcriptional activators or repressors, histone methyl- or acetyl-transferases, etc.

Importantly, ECs enable a functional decoupling of pharmacokinetics (PK) and pharmacodynamics (PD), allowing effects on gene transcription to long outlast the duration of drug exposure. Optimized mRNA drug product is delivered via LNP, translated EC protein modulates epigenetic state, and then EC protein and mRNA degrades

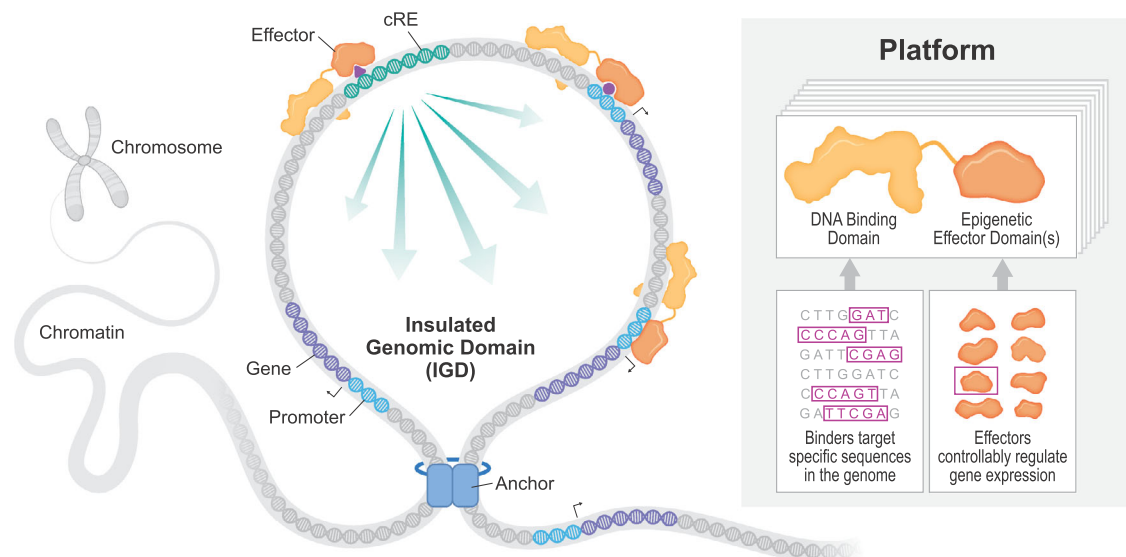


Fig. 1 | A systematic approach to precision epigenomic control. Gene transcription is controlled by elements such as promoters, cis-Regulatory Elements (cREs), and anchors within Insulated Genomic Domains. A systematic approach based on a library of Epigenomic Controllers (ECs) allows precision control of gene programs through modulation of epigenetic state. Briefly, epigenomic effectors,

chosen from an in-house library, are fused to customized DNA binding domains to form ECs. These ECs target specific elements that control transcription and can be applied to induce a tuned transcriptional response of one or multiple Insulated Genomic Domain (IGD) genes.

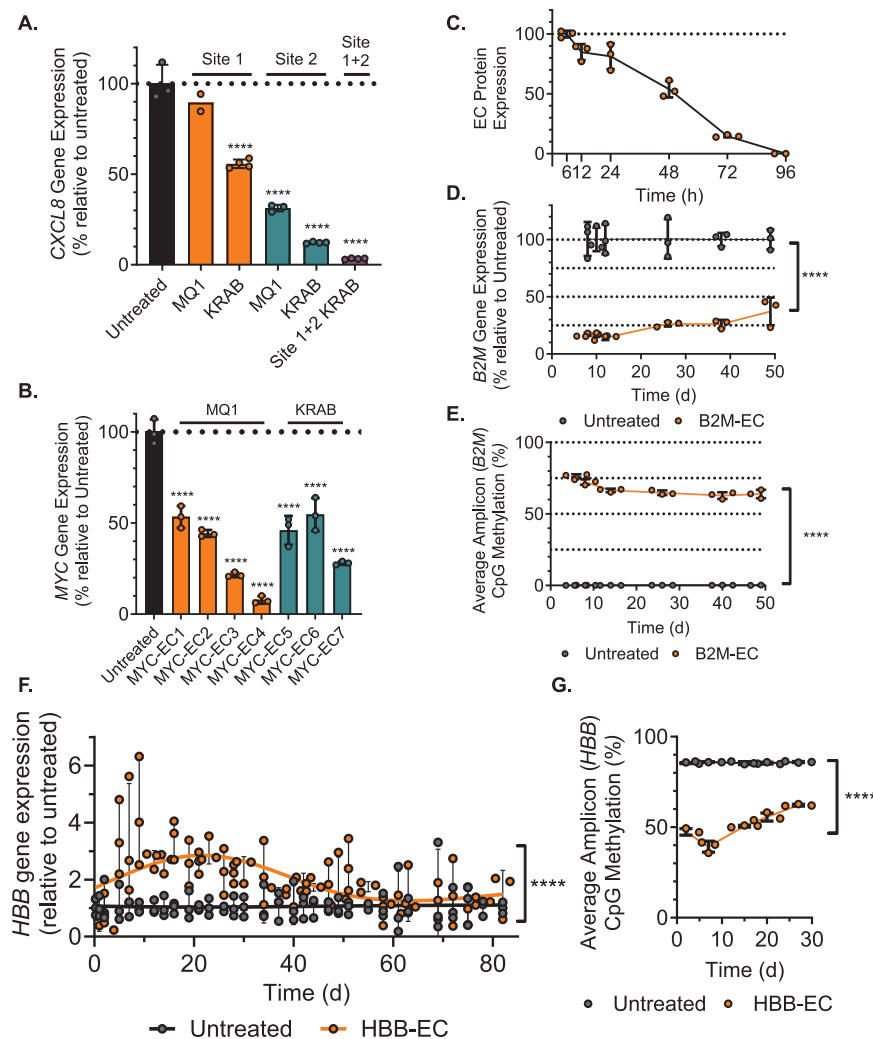


Fig. 2 | Epigenomic controllers demonstrate tunable, durable effects with decoupled PK and PD in vitro. **A** Transfection of IMR90 cells stimulated with IL1A with different effectors shows better 48 h downregulation of *CXCL8* gene expression with KRAB ($n = 3$) compared to MQ1 ($n = 2$) when targeting the *CXCL8* cis-regulatory Element (cRE, Site 1, orange, 45% vs. 11%) or promoter (Site 2, teal, 88%, $n = 4$, vs. 69%, $n = 3$). A combination therapy that targets both sites using a KRAB effector shows 95% *CXCL8* downregulation (purple, $n = 4$; **** $P < 0.0001$, one-way ANOVA). **B** Hep3B cells treated with MQ1 (orange) or KRAB (teal) effectors targeting distinct DNA elements at *MYC* (MYC-EC1 through MYC-EC7, $n = 3$ per group) show a wide range of *MYC* gene expression inhibition, between 50% and 90% compared to control untreated cells (black, $n = 3$ per group; **** $P < 0.0001$, one-way ANOVA). **C** B2M-EC protein expression levels in K-562 cells reduce to undetectable levels by 96 h post-transfection. The results are from 3 biological replicates. **D** Treated cells (orange, $n = 3$ per timepoint) maintain *B2M* gene expression

downregulation over 49 days compared to control untreated cells (black, $n = 3$ per timepoint; **** $P < 0.0001$, t test). **E** *B2M* promoter methylation was detected in B2M-EC treated K-562 cells with 64% methylation at 49 days (orange), whereas the *B2M* promoter remained unmethylated (<1%) in untreated cells (black); plotted values represent mean CpG methylation across the amplicon from 3 biological replicates per group and timepoint \pm standard deviation (SD; **** $P < 0.0001$, t test). **F** HBB-EC treatment (orange, $n = 3$ per timepoint) upregulates *HBB* gene expression in K-562 cells over 82 days compared to control (black, $n = 3$ per timepoint; **** $P < 0.0001$, t test). **G** HBB-EC treated K-562 cells show decreased *HBB* promoter methylation (orange) compared to untreated cells (black) through 28 days; plotted values represent mean CpG methylation across the amplicon from 3 biological replicates per group and timepoint \pm SD (**** $P < 0.0001$, t test). For all relevant panels, error bars represent mean \pm SD across the sample size, n , indicating biological replicates from independent experiments. Source data are provided as a Source Data file.

within days. The biological effect can last weeks or months after the drug product degrades for a potentially improved safety profile.

Here, we describe a platform for controlled epigenomic modulation of gene expression that is targeted, tunable, and durable. We demonstrate the utility of this platform through targeted epigenomic regulation of the *CXCL1-8* genomic locus, a critical axis in the inflammatory response pathway.

Results

Epigenomic controllers demonstrate tunable, durable effects in vitro with decoupled PK and PD

Epigenomic controllers can target different levels of gene expression and durability of effect through multiple design strategies. This

includes the choice of which non-coding elements to target, the selection of effector domains, and nucleotide-level optimizations driving genomic DBD binding. To demonstrate levels of tunability, we employed a tool system with mRNAs encoding effector proteins fused to dCas9 which were then co-transfected with sgRNA targeting unique genomic sequences. First, we targeted two separate non-coding elements that regulate *CXCL8* expression within the *CXCL1-8* IGD. By applying different effectors (a DNA methyltransferase MQ1 and the Kruppel-associated box domain KRAB) at each site, we observed distinct transcriptional inhibition levels for each effector/target combination (Fig. 2A). Next, when co-transfecting sgRNA targeting both non-coding sites along with dCas9-KRAB, we observed additive effect (Fig. 2A). To enable control at multiple expression level targets,

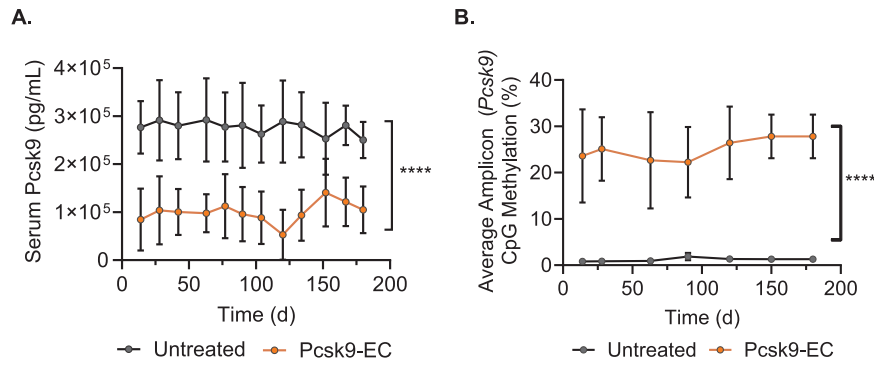


Fig. 3 | Epigenomic controllers maintain durable repression in vivo. **A** In C57BL/6 female mice, a single 3 mg/kg dose of Pcsk9-EC led to a reduction in Pcsk9 serum levels (orange) compared to control mice (black) as measured by ELISA for up to 180 days. Serum was sampled every 14 days post-treatment ($n = 10$ mice in each

cohort, **** $P < 0.0001$, t test). **B** Pcsk9 promoter methylation was increased in liver punches from Pcsk9-EC treated mice (orange) compared to control mice (black) up to 180 days post-treatment ($n = 10$ mice in each cohort; **** $P < 0.0001$, t test). Source data are provided as a Source Data file.

Table 1 | Long-term significant differential methylated regions in Pcsk9-EC treated mice after 6 months

Positions	Gene	Gene Region	DMR width (bp)	β
chr4:106463890-106463987	<i>Pcsk9</i>	PP	98	0.822
chr4:106464483-106465223	<i>Pcsk9</i>	PP	741	0.839
chr4:106464075-106464187	<i>Pcsk9</i>	PP	113	0.607
chr4:106463708-106463803	<i>Pcsk9</i>	PP	96	0.728
chr13:57908322-57908349	<i>Spock1</i>	PP	28	0.547
chr16:10823600-10823995	NA	Intergenic	396	-0.731
chr8:22508763-22508933	<i>Slc20a2</i>	Intronic	171	0.770

PP Promoter-proximal, Intronic: non-regulatory region.

different effectors were directed to different loci within an IGD: two distinct non-coding elements that regulate *MYC* expression within the *MYC* IGD using ZFP-like DBDs tethered to either MQ1 or KRAB. Within each non-coding region, binding location and affinity were varied through the selection of different ZFP-like DBDs, resulting in tuned downregulation of *MYC* (Fig. 2B). By integrating knowledge of non-coding regulatory elements, epigenetic state, and precise controller binding, we can model epigenomic targeting strategies across a wide range of desired expression level change.

ECs decouple PK and PD dynamics, offering a potentially improved safety profile wherein the administered drug product and translated protein EC(s) degrade in a matter of days while gene expression change can persist via natural epigenetic mechanisms for weeks to months. This decoupling is enabled by “hit-and-run” kinetics, where the deposition of epigenetic marks persists and continues to modulate gene expression long after EC degradation^{13,14}. To demonstrate this decoupling in vitro we targeted the CpG island of the *B2M* promoter in K-562 cells with an epigenetic controller, B2M-EC, comprised of a ZFP-like DBD tethered to MQ1. Expression of B2M-EC was observed within 6h (Fig. 2C) along with a -85% decrease in *B2M* expression (Fig. 2D). We observed a concomitant -75% increase of DNA methylation at the target site (Fig. 2E), indicating successful epigenetic transcriptional regulation. Inhibition of *B2M* expression, along with on-target DNA methylation, was maintained 49 days after a single EC treatment, at which point culture conditions began to deteriorate, whereas controller expression was undetectable within 4 days after treatment.

We demonstrate durable up-regulation by targeting the CpG island at the *HBB* gene in K-562 cells with an epigenetic controller, HBB-EC, containing a TAL-like DBD tethered to a methylcytosine dioxygenase TET2¹⁵. We observed a -4.3-fold up-regulation of *HBB* gene expression 9 days after treatment, with -1.7-fold up-regulation

maintained through 55 days (Fig. 2F). Demethylation of the target region was confirmed by amplicon methylation sequencing (Fig. 2G) with peak demethylation observed 7 days post-treatment.

To extend our proof of concept of epigenomic control to an in vivo setting, we designed Pcsk9-EC, a TAL-like DBD tethered to MQ1, targeting the promoter of the murine *Pcsk9* gene. Pcsk9 is a secreted protein that plays a key role in cholesterol homeostasis¹⁶ and whose inhibition can be monitored longitudinally via serum Pcsk9 protein levels, thus presenting an ideal testing scenario to examine EC durability. Pcsk9-EC induced near-complete inhibition in Hepa1-6 cells in vitro, and it demonstrated dose-responsive levels of serum Pcsk9 reduction in a pilot murine in vivo study seven days after treatment using a tool LNP (Supplementary Fig 1). An in vivo study was conducted by treating C57BL/6 mice with a single 3 mg/kg dose of Pcsk9-EC and then sampling serum every 14 days out to 6 months post-treatment. Mouse cohorts were sacrificed at monthly time points to examine liver tissue for on-target DNA methylation. Pcsk9-EC robustly inhibited serum Pcsk9 throughout study duration, without any diminution of effect out to 6 months (Fig. 3A), which correlated with an on-target increase in DNA methylation in liver throughout (Fig. 3B). Pcsk9-EC was well tolerated without any significant weight loss observed compared to PBS-treated control mice (Supplementary Fig 2) and did not exhibit any obvious liver tissue damage.

To understand the genomic specificity of the EC effect in vivo, we performed whole-genome methylation sequencing (WGMS) on gDNA extracted from Pcsk9-EC treated whole liver tissue along with 3'mRNA sequencing. When comparing all Pcsk9-EC treated animals to PBS-treated controls, modeling timepoint data as a covariate for increased power, we identified 4 differentially methylated regions (DMRs) (adj. $p < 0.05$, Table 1). These DMRs indicate loci that sustain methylation change throughout the entirety of the 6-month treatment duration and include the *Pcsk9* promoter as a top hit, the specific target of

Pcsk9-EC and recapitulating the amplicon methylation sequencing data. *Spock1*, an extracellular matrix proteoglycan, and *Slc20a2*, a sodium-phosphate transporter, both with little known relationship to disease, showed increased methylation at their promoter and intron, respectively. The final significant DMR was an intragenic region with a decrease in DNA methylation in treated animals compared to controls, a change incongruent with the known mechanism of the direct Pcsk9-EC effect. Differential gene expression analysis using 3' mRNA sequencing showed that only *Pcsk9* (adj. $p = 7.36 \times 10^{-6}$, $\log_2 \text{FC} = -1.08$) and *Cd163*, a macrophage scavenger receptor associated with anti-inflammation were significant (adj. $p = 1.16 \times 10^{-7}$, $\log_2 \text{FC} = -1.39$, Table 2) after controlling for time. Neither *Spock1* nor *Slc20a2* showed significant differences in expression. These in vivo data, identifying *Pcsk9* as the sole gene with both epigenetic and transcriptional effects, indicate high specificity for the Pcsk9-EC over 6 months.

Finally, by acting on chromatin pre-transcriptionally, engaging only two alleles per cell instead of thousands of molecular substrates (mRNA, protein), epigenomic controllers offer fundamentally different dose-response profiles than other therapeutic modalities such as small molecules and siRNA. This may offer the potential for high potency with dramatically lower drug exposure and improved safety profile. To examine the molecular kinetics underlying our pharmacodynamic dose response at the single-cell level, we built a fluorescence-based system where epigenomic controller delivery and target engagement directly result in an optical signal that allows for sorting by flow cytometry. Specifically, we made a CRISPR-based knock-in K-562 cell line that couples the expression of a destabilized GFP variant (d2GFP) to *MYC* expression (K-562 MYC/d2GFP)^{17,18} (Supplementary Fig. 3A). We also designed a bicistronic epigenomic controller mRNA, which targets the *MYC* promoter (using a ZFP-like DBD coupled to MQ1) but co-expresses fluorescent tdTomato protein via a 2A self-cleaving peptide¹⁷ (MYC-EC). Treatment of the engineered cell line with the small molecule BET inhibitor JQ1^{19,20}, known to downregulate *MYC* transcription,

showed an expected dose-dependent decrease in d2GFP expression indicated by progressive, continuous shifts in fluorescence intensity. In contrast, titration of MYC-EC dose downregulates *MYC* in a more bimodal fashion, with a roughly constant population shift associated with *MYC* inhibition across tested doses (Fig. 4A). MYC-EC treated cells were further sorted into populations indicating functional delivery (d2GFP+/dTomato+) or lack of delivery (d2GFP+/dTomato-). The functional delivery positive group showed 96% methylation at the *MYC* promoter, while the functional delivery negative group had less than 1% methylation (Fig. 4B). Analysis of matched bulk cells showed 64% methylation. These data suggest a model whereby lack of gene modulation may be attributable solely to lack of functional delivery. Thus, epigenomic controllers are capable of avoiding the pharmacodynamic challenges of prior modalities, impacting therapeutic dose selection.

Simultaneous epigenomic control of *CXCL1-8* locus

Using our platform, we designed an epigenomic controller that inhibits the entire *CXCL1-8* multi-gene cluster (Fig. 5A) using a single mRNA, preventing dysregulation under inflammatory or stimulatory conditions and directly impacting neutrophil migration. With the potential to be used in multiple different indications depending on the location of inflammation, this target set highlights the benefit of modular EC drug development. For example, when paired with a clinical grade LNP with lung tropism, this controller could lead to an effective therapeutic for ARDS, but a combination with a skin-specific delivery vehicle could be used instead to treat psoriasis. While NF- κ B inhibition is a common anti-inflammation strategy, we took a unique approach by inhibiting specific cytokine overproduction only at the *CXCL1-8* locus, targeting two genomic regulatory sites within the IGD that mediate NF- κ B P65-induced *CXCL1-8* upregulation²¹. We modeled the epigenetic state, transcription factor occupancy, and accessibility of the *CXCL1-8* IGD and validated P65 binding at a key cRE upstream of *CXCL8* as well as at the *CXCL8* promoter using ChIP-seq (Fig. 5A, I).

We first designed CXCL-EC₁, a TAL-based DBD coupled to a KRAB-based effector that directly targets the *CXCL8* promoter. Pre-treating IMR90 cells with CXCL-EC₁, followed by stimulation by IL1A, demonstrated a 99% reduction in *CXCL8* expression compared to the control, (Fig. 5B). However, when only targeting the *CXCL8* promoter, we observed a concomitant IL1A-dependent increase in the expression of *CXCL1/2/3* (Fig. 5B), suggesting potential compensation of these functionally related cytokines under high downregulation of *CXCL8*,

Table 2 | Time adjusted significant differential expression genes in Pcsk9-EC treated mice after 6 months

Gene	Ensembl ID	log2 Fold Change	Adj. P-value
<i>Cd163</i>	ENSMUSG00000008845	-1.39	1.16E-07
<i>Pcsk9</i>	ENSMUSG00000004254	-1.08	7.36E-06

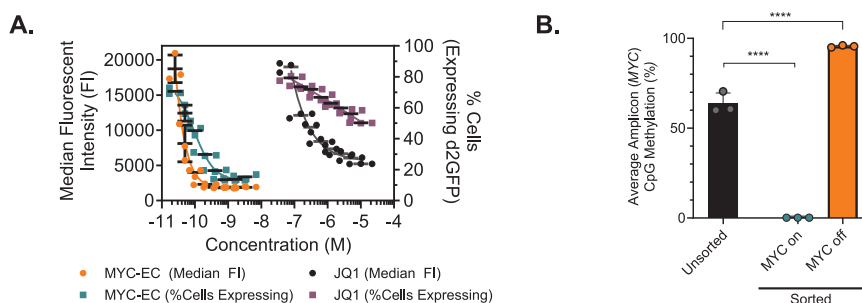


Fig. 4 | Kinetics of EC-driven transcriptional repression of the *MYC* locus.

A Dose-response analysis of pharmacodynamic transcriptional repression of the *MYC* locus at the bulk level using median fluorescence intensity (FI) or at the single cell level by categorizing cells as “expressing” or “downregulated” reflected these differential kinetics as steeper Hill coefficients in MYC-EC treated conditions. Flow cytometric analysis of K-562 MYC/d2GFP cells treated with MYC-EC or JQ1 using four-parameter logistic regression shown. Median FI in MYC-EC treated cells (orange) reaches a lower best-fit bottom of 1800 compared to JQ1 treated cells (5549; black) with a steeper HillSlope (-1.724 vs. -0.7816 ; $P = 0.0004$, F-test). Using GFP as a gate to classify cells as transcriptionally active or repressed at the *MYC* locus, MYC-EC treatment (teal) results in a steeper HillSlope compared to JQ1 treatment (purple; -1.406 vs. -0.0398 ; $P = 0.0008$, F-test). Plotted values represent

the mean of three biological replicates \pm standard deviation (SD). FACS gating strategy depicted in Supplementary Fig. 3B and C. **B** Amplicon methylation sequencing was used to assess *MYC* promoter methylation in K-562 MYC/d2GFP cells treated with $0.625 \mu\text{g/ml}$ MYC-EC for 44 h. The unsorted cells showed an average CpG methylation across the amplicon of 64% (black), whereas 96% of CpGs in the amplicon were methylated after sorting for functionally delivered cells (orange, GFP+/tdTomato+). 1% of CpGs were methylated in the amplicon in untransfected, MYC On cells (GFP+/tdTomato-). Plotted values represent mean CpG methylation across the amplicon \pm SD from 3 technical replicates (**** $P < 0.0001$, one-way ANOVA). FACS gating strategy depicted in Supplementary Fig. 4. Source data are provided as a Source Data file.

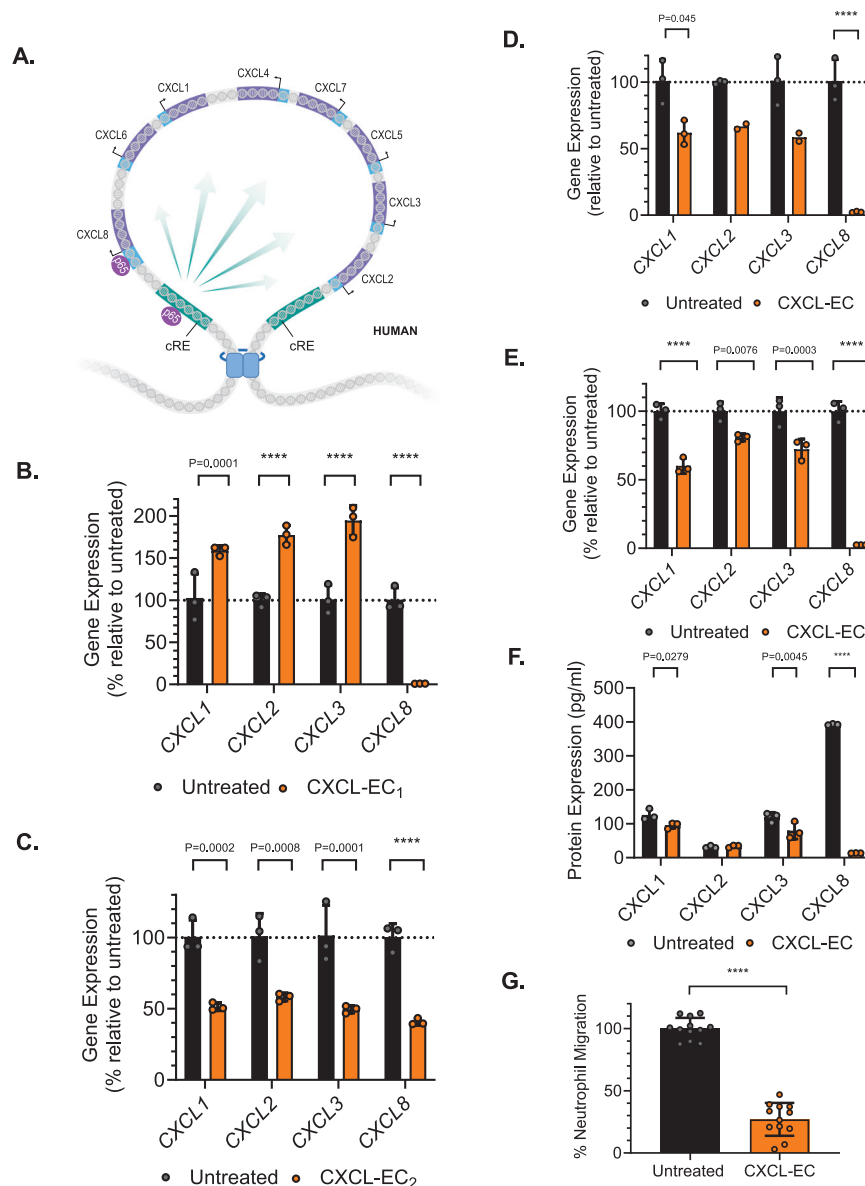


Fig. 5 | Simultaneous epigenomic control of *CXCL1-8* locus leads to reduced neutrophil migration in vitro. **A** Schematic depiction of the looping at the human *CXCL1-8* locus. Genes, anchors, and P65-related cis-regulatory elements (cRE) indicated. **B** IMR90 cells stimulated with IL1A and treated with CXCL-EC₁ (orange, *n* = 3 per group) targeting the *CXCL8* promoter show a 99% reduction in *CXCL8* expression and increased *CXCL1/2/3* expression compared to control (black, *n* = 3 per group; *****P* < 0.0001, one-way ANOVA). **C** When treated with CXCL-EC₂ targeting the upstream cRE (orange, *n* = 3 per group), IMR90 cells have a 45–60% reduction in *CXCL1/2/3/8* expression compared to control (black, *n* = 3 per group; *****P* < 0.0001, one-way ANOVA). **D** When treated with CXCL-EC targeting both elements (orange), IMR90 cells show a 98% reduction in *CXCL8* compared to control (black, *n* = 3, *****P* < 0.0001, one-way ANOVA) and a 39% reduction in *CXCL1* compared to control (*n* = 3, *p* = 0.0045, one-way ANOVA). We observed a 33% and 42% reduction in *CXCL2* and *CXCL3*, respectively, in CXCL-EC treated cells (*n* = 2) when compared to control (black). **E** Primary Asthma Lung Fibroblasts (PALF) were stimulated with IL1A and treated with CXCL-EC (orange, *n* = 3 per group), resulting

in 98% reduction in *CXCL8* gene expression (*****P* < 0.0001, one-way ANOVA), 40% inhibition of *CXCL1* expression (*****P* < 0.0001, one-way ANOVA), 19% reduction of *CXCL2* expression (*P* = 0.0076, one-way ANOVA), and 28% inhibition of *CXCL3* gene expression (*P* = 0.0003, one-way ANOVA) compared to control. **F** In PALF, IL1A stimulates CXCL1, CXCL3, and CXCL8, protein expression as measured by ELISA, to 126 pg/ml, 119 pg/ml, and 392 pg/ml, respectively (black, *n* = 3). EC treatment (orange, *n* = 3) led to a 24% downregulation of CXCL1 (*P* = 0.0279, one-way ANOVA), a 33% downregulation of CXCL3 (*P* = 0.0045, one-way ANOVA), and a 97% downregulation of CXCL8 (*****P* < 0.0001, one-way ANOVA). **G** In a Boyden chamber assay, neutrophil migration was reduced by 73% when exposing cells from human plasma donors (*n* = 12) to supernatant from CXCL-EC treated IMR90 cells (orange) compared to supernatant from control cells (black; *****P* < 0.0001, one-way ANOVA). For all relevant panels, error bars represent mean ± standard deviation (SD) across the sample size, *n*, indicating biological replicates from independent experiments. Source data are provided as a Source Data file.

and supporting the potential need for IGD-wide downregulation to achieve the therapeutic effect. A second controller was designed, CXCL-EC₂, a ZFP-based DBD coupled to a KRAB-based effector that targeted the identified upstream cRE. Pre-treating IMR90 cells with CXCL-EC₂, followed by stimulation by IL1, led to a 45–60% reduction in *CXCL1/2/3/8* expression compared to the control, (Fig. 5C). For

combined effect, a bicistronic mRNA encoding CXCL-EC₁ and CXCL-EC₂ (together, CXCL-EC), was developed and tested in IMR90 (Fig. 5D) leading to 30–95% reduction expression across the *CXCL1-8* IGD, and in ARDS-relevant primary cells using the same assay. In human Asthma lung fibroblasts, CXCL-EC led to a 20–97% reduction in expression across the *CXCL1-8* IGD at the mRNA (Fig. 5E) and protein levels

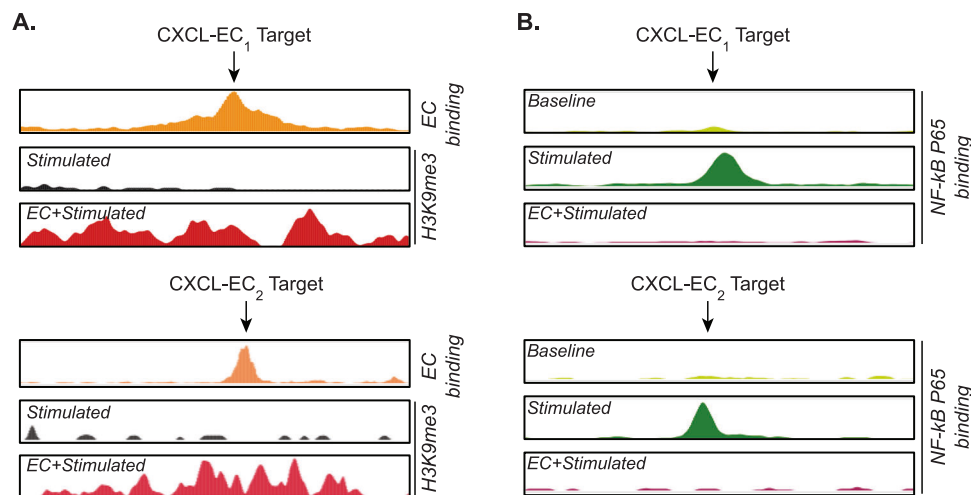


Fig. 6 | ChIP-seq confirms on-target chromatin association and epigenetic modifications. **A** HA ChIP-seq (orange) identifies on-target EC-chromatin association at the *CXCL8* promoter (top) for CXCL-EC₁ and at the upstream cRE (bottom) for CXCL-EC₂. H3K9me3 ChIP-seq shows an establishment of the inhibitory signature mark at each locus after EC treatment (red) that is absent in control

stimulated, untreated cells (black). **B** CXCL-EC₁ and CXCL-EC₂ treatment leads to a depletion of NF-κB binding at the *CXCL8* promoter (top) and cRE (bottom) targets after stimulation (purple). Results are from 2 biological replicates from independent experiments.

(Fig. 5F). Notably, the least impacted chemokine in this cluster was CXCL2, which could be attributed to the low absolute protein expression even in the presence of IL-1A stimulation.

To assess phenotypic impact in vitro, a neutrophil chemotaxis assay was used to quantify cell-level functional response given CXCL-EC treatment in an inflammation model. Human donor neutrophils were exposed to treated IMR90 cell supernatant using a Boyden chamber, permitting quantification of neutrophil migration. Across the six different donors examined, we observed a 60–80% decrease in neutrophil migration compared to controls exposed to untreated IMR90 cell supernatant, demonstrating a robust reduction of a key inflammation process (Fig. 5G).

To validate the molecular targeting strategy of CXCL-EC, a multi-gene CXCL1-8 IGD inhibitor that operates in part through specific targeting of the NF-κB P65 binding sites, we designed HA-tagged versions of CXCL-EC₁ and CXCL-EC₂ and validated target engagement and epigenetic modification. Using HA-ChIP-seq in the same IMR90 stimulation assay, on-target controller/chromatin binding is observed at each of the target non-coding elements (Fig. 6A, top), along with the establishment of the inhibitory chromatin signature H3K9me3 only after EC treatment (Fig. 6A, bottom). Functionally, onset of NF-κB P65 binding is seen following stimulation, driving *CXCL1-8* upregulation, however these sites are refractory to P65 binding upon EC treatment (Fig. 6B).

Identification of functionally homologous *CXCL1-8* epigenetic targeting approach in mouse

Due to the limited translatability of human models for ARDS, a mouse model of acute lung injury which induces a neutrophilic inflammatory response was utilized to demonstrate in vivo efficacy. In the mouse, the genes encoding IL-8 and CXCR1 have no evolutionary homolog²²; with *Cxcl1* and *Cxcl2* performing functionally similar roles in their binding of the *Cxcr2* receptor during inflammatory processes^{23,24}. Additionally, there has been no direct syntenic homolog to the cRE targeted by CXCL-EC₂, which exerts IGD-wide regulatory control, previously identified in mouse. A surrogate epigenomic controller was developed to downregulate both homologous murine genes, *Cxcl1* and *Cxcl2*, and assess potential therapeutic benefits in disease models.

We first validated that upon stimulation, *Cxcl1* overexpressed with P65 bound to the promoter, as seen with *CXCL8* in humans. An epigenomic controller, MM-Cxcl-EC₁, was designed to target the *Cxcl1*

promoter using a TAL-based DBD and KRAB-based effector. Pre-treatment of MM-Cxcl-EC₁ in NIH3T3 cells, followed by stimulation by IL1, led to an 80% reduction of *Cxcl1* mRNA compared with control (Fig. 7B). Second, we sought to identify a functionally homologous cRE with the ability to control IGD-wide expression based on epigenetic mapping of the murine locus. H3K27ac- and P65-ChIP-seq were performed on NIH3T3 cells, revealing a putative homologous cRE upstream of *Cxcl5* engaging NF-κB (Fig. 7A). A surrogate epigenomic controller was designed to target this site, MM-Cxcl-EC₂, a dCas9-based DBD protein with a matched KRAB-based effector. Pre-treatment of MM-Cxcl-EC₂ in NIH3T3 cells, followed by stimulation by IL1, led to 40–60% expression reduction of both *Cxcl1* and *Cxcl2* (Fig. 7C). Co-formulation of MM-Cxcl-EC₁ and MM-Cxcl-EC₂ assayed in the same system led to 87% expression reduction of *Cxcl1* and 50% of *Cxcl2* (Fig. 7D), closely mirroring the human bicistronic CXCL-EC in form, mechanism, and function.

Epigenetic controllers demonstrate in vivo therapeutic response in a mouse asthma model

To examine the therapeutic potential of epigenomic controllers to moderate immune response in vivo, we tested the anti-inflammatory benefit of the co-formulation of MM-Cxcl-EC₁ and MM-Cxcl-EC₂ in a mouse model of asthma. A hallmark feature of asthma is airway obstruction involving elevated levels of inflammatory cells, mucus production, bronchial hyperactivity, and airway remodeling and narrowing²⁵. Characterization of bronchoalveolar lavage fluid (BALF) has successfully elucidated the airway pathology of asthma and the action of anti-inflammatory drugs on the airway²⁶.

For this study, we screened LNPs to identify a tool lung-targeted agent that delivers ECs to mouse lungs. In vivo imaging (IVIS) of organs extracted from Ai14 reporter mice²⁷ dosed with *Cre* mRNA loaded into the LNP used in this study showed expression of the tdTomato reporter protein exclusively in the lungs when compared to major LNP accumulation organs, such as liver and spleen (Supplementary Fig. 4A). Using immunohistochemistry (IHC) to identify tdTomato protein at a cellular level, macrophages and airway epithelial cells showed the highest expression among the cell types identified in the lung (Supplementary Fig. 4B).

We evaluated the dynamic changes in immune responses under homeostatic and disease states upon LPS challenge by performing immunophenotyping with multicolor flow cytometry panels in BALF

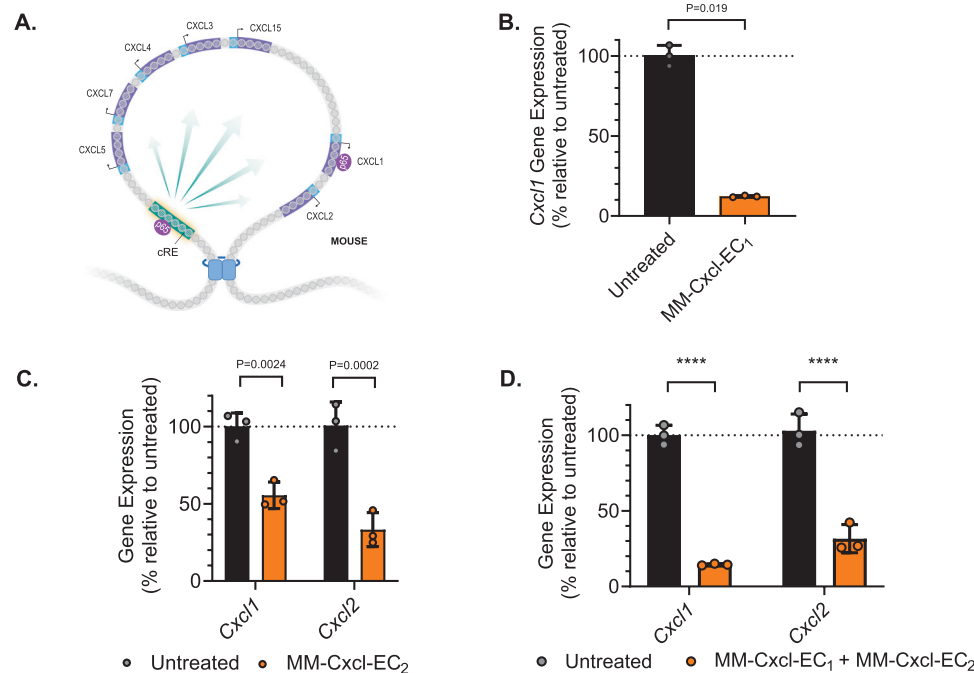


Fig. 7 | In vitro identification of a functionally homologous CXCL1-8 epigenetic targeting approach in mouse. **A** Schematic depiction of looping at the homologous mouse *Cxcl* locus. Genes, anchors, and P65-related cis-regulatory elements (cREs) indicated. **B** In vitro treatment of NIH3T3 cells with MM-Cxcl-EC₁ followed by LPS stimulation leads to the downregulation of *Cxcl1* gene expression by 88% (orange, $n = 3$) compared to LPS stimulation alone (black) ($n = 3$; $P = 0.0019$, one-way ANOVA). **C** Treatment with MM-Cxcl-EC₂ followed by LPS stimulation (orange, $n = 3$) leads to the downregulation of *Cxcl1* gene expression by 51% ($P = 0.0024$, one-

way ANOVA) and *Cxcl2* gene expression by 67% ($P < 0.0002$, one-way ANOVA) in NIH3T3 cells compared to LPS stimulation alone (black, $n = 3$). **D** Treatment with a combination of MM-Cxcl-EC₁ and MM-Cxcl-EC₂ followed by IL1A stimulation (orange, $n = 3$) leads to the downregulation of *Cxcl1* gene expression by 86% and *Cxcl2* gene expression by 71%, respectively, in NIH3T3 cells compared to IL1A stimulation alone (black, $n = 3$; **** $P < 0.0001$, one-way ANOVA). For all relevant panels, error bars represent mean \pm standard deviation (SD) across the sample size, n , indicating biological replicates. Source data are provided as a Source Data file.

samples. Dexamethasone (DEX), a synthetic glucocorticoid used for the treatment of inflammatory disorders, was used as a positive control. Identification and quantification of pulmonary myeloid cell subsets in conjunction with a lymphocyte phenotyping panel provided a broad characterization of pulmonary immune cell composition in this study. A single prophylactic 1 mg/kg intravenous administration of the MM-Cxcl-EC₁/MM-Cxcl-EC₂ co-formulation 8 h prior to LPS challenge significantly inhibited neutrophil recruitment into BALF 24 h post-LPS challenge when compared to LPS control alone (Fig. 8A). Although B-cells and T-cells commonly lack *Cxcr2* expression and would be thought to be unaffected by perturbation of *Cxcl1* signaling, we also observed concomitant inhibition of their recruitment into BALF (Fig. 8A). Since activated neutrophils are known to secrete other chemokines²⁸, we show here that selective inhibition of a key cytokine may have the potential to disrupt paracrine feedback loops to drive broad impact to the immune response in vivo.

In addition, we observed that EC treatment provided a protective effect from LPS-induced lung tissue damage. Morphologic pathology evaluation of lung tissue from treated and naïve mice showed that EC-treated animals had the mildest disease compared to control (Fig. 8B). We did not observe any changes in weight in the EC treated group relative to Dexamethasone or controls, indicating that a 1 mg/kg administration was well tolerated (Supplementary Fig. 5).

Importantly, by selectively inhibiting the *Cxcl* cluster from responding to NF- κ B signaling in the lung, while not interfering with other essential NF- κ B-related processes across the genome, we avoid the dangers of agents with pan- and/or systemic NF- κ B inhibition, which has been previously reported to stimulate tumor growth in some cancer models by promoting an M2-like phenotype in tumor-infiltrating macrophages²⁹. These findings demonstrate that epigenetic controllers provide an anti-inflammatory benefit in the setting of

neutrophilic accumulation in the respiratory tract, important in multiple respiratory diseases.

Discussion

Precision epigenomic therapies may fulfill the potential of early epigenetic approaches that, despite potent effects, were plagued by poor pharmacokinetic and safety/tolerability profiles^{5,30}. We describe a platform that enables the rapid design and development of programmable mRNA therapeutics enabling precise and durable epigenomic control – achieving the targeted specificity of CRISPR and other gene editing approaches without permanent changes to target cell DNA. Epigenomic controllers offer potent pre-transcriptional control of one or many genes, durably demonstrated up to 6 months. While epigenetic modulation using dCas9 systems have been reported previously³¹ and can rapidly facilitate screening efforts, their therapeutic application in vivo faces potential challenges related to delivery, production, immunogenicity, and pharmacodynamics. Furthermore, these systems cannot effectively control multiple genes to varying tunable levels and direction (i.e., up- and down-regulation) with a single therapeutic.

Safety remains a paramount concern for any therapeutic. We show here that with LNP delivery, ECs are well-tolerated in animal models without impacting body weights or causing any obvious tissue damage. ECs are selective in vivo, as shown by whole-genome methylation and whole-transcriptome profiling of the Pcsk9-EC, where potential off-target activity was limited to two genic regions without gene expression effect. Coupled with tissue-specific LNP delivery, ECs have the potential to avoid on-target toxicities and side effects that may arise from a systemic therapeutic that impacts all cell types, as commonly observed with oncology agents that are often dose-limited by the toxicities observed in hematopoietic and gastrointestinal cell compartments.

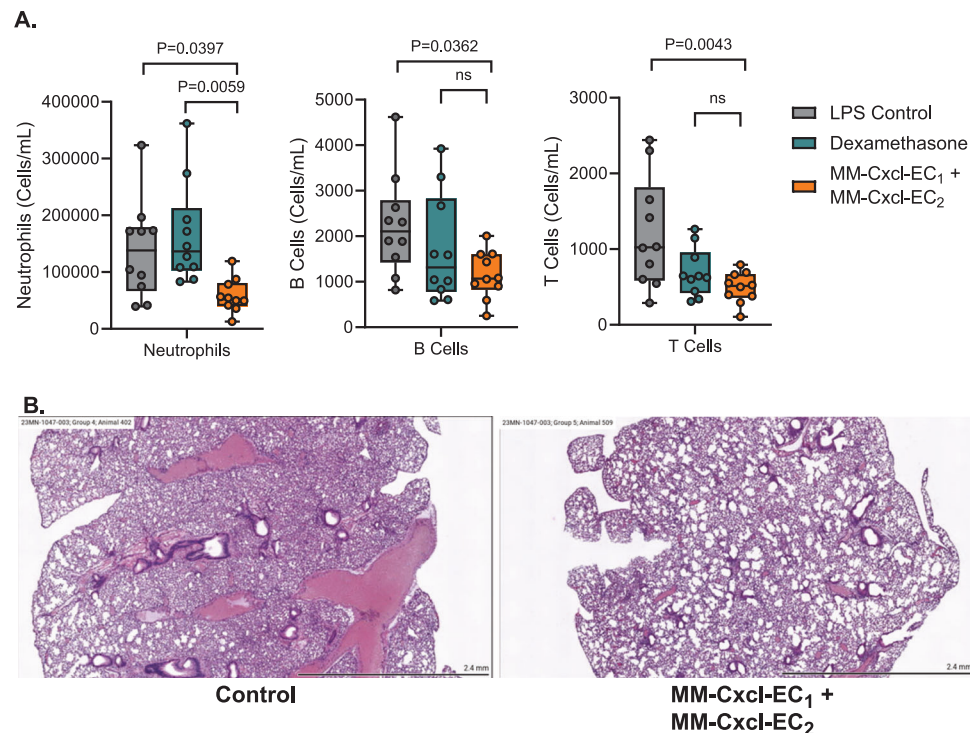


Fig. 8 | Epigenetic controllers (ECs) demonstrate in vivo therapeutic response in a mouse asthma model. A Immune cell recruitment into bronchoalveolar lavage fluid (BALF) was reduced following a single prophylactic 1 mg/kg administration of the MM-Cxcl-EC₁/MM-Cxcl-EC₂ co-formulation 8 h prior to lipopolysaccharide (LPS) challenge. Based on immune cell phenotyping by flow cytometry 24 h post-LPS challenge, EC treatment (orange) inhibited recruitment of neutrophils (CD45 +, Siglec F-, CD11b +, CD11c-, Ly-6G +) compared to LPS challenge alone (gray) by 58% ($P=0.0397$, one-way ANOVA) and Dexamethasone controls (teal) by 65% ($P=0.0059$, one-way ANOVA). B-cell (CD45 +, Siglec F-, CD11c-, B220 +) and T-cell

(CD45 +, Siglec F-, CD11c-, CD3 +) recruitment were also inhibited compared to LPS challenge alone by 49% ($P=0.0362$, one-way ANOVA) and 59% ($P=0.0043$, one-way ANOVA), respectively. Boxplots represent data from $n=10$ mice from one independent experiment, depicting the maximum, 3rd quartile, median, 1st quartile, and minimum. **B** Pathologist scoring of lung tissue immunohistochemistry (IHC) sections shows a reduction in lung injury from EC treatment compared to controls after the LPS challenge. Representative sections of GFP-treated control (left) and EC-treated (right) lungs are shown. Source data are provided as a Source Data file.

This coupling between genomic and cell-type specificity highlights the importance of a delivery system that is appropriate for clinical applications³². In the in vivo studies shown here, we demonstrate on-target tissue delivery of ECs using tool LNPs, while clinical LNPs remain the focus of active development³³. LNPs are well suited for epigenomic mRNA therapeutics because this pairing enables decoupled PK/PD, conferring durable gene control with only transient potential drug product side effects. In addition, LNPs allow redosability, enabling the evaluation of a variety of therapeutically beneficial dosing regimens³⁴. Further, the maturity of LNP technology and CMC production knowledge, and its well characterized safety profiles, allows for straightforward clinical development paths^{35,36}.

Using this platform we rationally designed a controller (CXCL-EC) that downregulates expression of the *CXCL1-8* gene cluster. Treatment with co-formulated murine surrogates, based on the identification of functional regulator element homologs, shows therapeutic anti-inflammatory efficacy in a mouse model of asthma, suggesting the potential therapeutic utility of CXCL-EC in autoimmune disease and multiple inflammatory indications, including pulmonary applications such as neutrophilic asthma. We show here that by considering all potential non-coding regulatory elements at targets, mediated by IGD biology, homeostatic expression levels can be corrected through single or multi-targeting of epigenetic state. ECs offer a unique ability to impact disease known to be driven by multiple underlying genes, as well as target genes previously considered “undruggable.”

Methods

Ethical Statement

The protocols used for the Pcsk9-EC animal study, MM-Cxcl-EC animal study, and LNP biodistribution study were reviewed and received ethical approval from the Pharma Models (Marlborough, MA), MLM Medical Labs (Minneapolis, MN), and Biomere Biomedical Research Models, Inc. (Worcester, MA) Institutional Animal Care and Use Committees (IACUC), respectively. Animal studies were performed by Pharma Models, MLM Medical Labs, or Biomere in the presence of an attending veterinarian at the facility, as necessary, and all animal welfare concerns were addressed and documented. Sex was not considered for the study design, as only female mice were used. Female mice were used for housing purposes. Therefore, disaggregated sex information was not necessary.

Design and production of epigenetic controller mRNA

Controllers were designed to target specific DNA sequences within genomic regulatory elements of interest in-house. Synthesis of the coding sequence of each controller was performed by ATUM (Newark, CA) and subcloned into the appropriate in vitro translation (IVT)-capable backbone vector. Plasmids were scaled up, and sequences were confirmed by Sanger sequencing prior to IVT. For mRNA production, plasmids were linearized with SapI and purified using a phenol:chloroform extraction. The linearized plasmid was then added to an in vitro transcription (IVT) reaction using a T7 RNA polymerase, unmodified NTPs, HEPES buffer, magnesium chloride, DTT, spermidine, RNase inhibitors, and pyrophosphatase at proprietary

concentrations. This reaction was incubated at 41 °C for 2 hours. This crude IVT mixture was then treated with DNase to digest the linearized plasmid, and the resulting mRNA was capped in an enzymatic reaction comprised of Hepes buffer, potassium chloride, DTT, GTP, SAM, RNase inhibitors, guanylyltransferase and 2-O-methyltransferase at proprietary concentrations at 37 °C for 1 h. This mixture was then purified using OligodT chromatography and eluted in molecular biology-grade water.

Preparation of LNPs for in-vitro transfection

Lipid nanoparticles were produced for in vitro transfection via microfluidic mixing using the NanoAssemblr™ Spark™ (Precision NanoSystems). mRNA encoding an Epigenomic Controller (EC) at 0.4 mg/mL in either 50 mM citric acid buffer, pH 4.5, or 50 mM malic acid buffer, pH 4.5, was mixed with an ethanolic lipid phase at Flow Rate Ratio = 3:1 (aqueous: organic). The ethanol phase contained either MC3 ((6Z,9Z,28Z,31Z)-heptatriacont-6,9,28,31-tetraene-19-yl 4-(dimethylamino)butanoate) or SS-OP (4-[(9Z)-1-oxo-9-octadecen-1-yl]oxy]-benzeneacetic acid, 1,1'-[dithiobis(2,1-ethanediy-1,4-piperidinediy-2,1-ethanediy)] ester) as the main ionizable lipid, cholesterol, DOPC (1,2-dioleoyl-sn-glycero-3-phosphocholine), and DMG-PEG2000 (1,2-dimyristoyl-rac-glycero-3-methoxypolyethylene glycol-2000) at 45:44:9:2 mole ratio. The ionizable-lipid-to-RNA mass ratios were 6:1 and 10:1 for MC3 and SSOP, respectively.

LNPs were collected in 3 volumes of 1X phosphate-buffered saline, pH 7.4 post-mixing to dilute ethanol content and allow for proper formation of the nanoparticles. The final mRNA concentration was adjusted with a cell culture medium immediately prior to transfection.

Preparation of LNPs for in vivo dosing in mice

Lipid nanoparticles were produced for dosing in mice via microfluidic mixing using the NanoAssemblr™ Ignite™ (Precision NanoSystems). mRNA encoding a reporter protein (Cre Recombinase) or an Epigenomic Controller (EC) at 0.25–1 mg/mL in 50 mM citrate buffer, pH 4.5 was mixed with an ethanolic lipid phase at Flow Rate Ratio = 2:1 (aqueous: organic).

For *Pcsk9* studies, the ethanol phase contained MC3 as the main ionizable lipid, cholesterol, DSPC (1,2-distearoyl-sn-glycero-3-phosphocholine), and DMG-PEG2000 (1,2-dimyristoyl-rac-glycero-3-methoxypolyethylene glycol-2000) at 50:38.5:10:1.5 mole ratio. The MC3-to-RNA mass ratio used was 6:1.

For biodistribution and *Cxcl* studies, the ethanol phase contained DOTAP as main cationic lipid (1,2-dioleoyl-3-trimethylammonium-propane), cholesterol, DOPC (1,2-dioleoyl-sn-glycero-3-phosphocholine), and DMG-PEG2000 (1,2-dimyristoyl-rac-glycero-3-methoxypolyethylene glycol-2000) at 45:45:9:1 mole ratio. The DOTAP-to-RNA mass ratio used was 6:1.

LNPs were dialyzed post-mixing against storage buffer (pH 7, 8–10% sucrose) for ethanol removal, following concentration by tangential flow filtration and sterile filtration prior to storage at –80 °C. LNP diameter ranged from 60–100 nm as measured by dynamic light scattering (Wyatt Mobius). RNA encapsulation was determined via RiboGreen assay to be above 90% for all LNPs produced.

In vitro transcriptional and protein read-outs

All cell lines, including NIH3T3 (ATCC #CRL-1658), IMR90 (ATCC #CCL-186), K-562 (ATCC #CCL-243), Hep3B (ATCC #HB-8064), and Hepa1-6 (ATCC #CRL-1830), were sourced from and authenticated by the ATCC and grown in a humidified 37 °C incubator with 5% CO₂. Cultures were routinely tested for mycoplasma contamination by PCR. Cells were not otherwise authenticated. Cells were transfected with LNPs containing controller mRNA, which was added to the media at a final concentration of 1 µg/mL of mRNA. After a 48 h incubation, IL1-alpha (PCH0015, Life Technologies) was added at 10 ng/mL final concentration, and the samples were incubated for 1 h. For protein,

supernatant was collected after a 1 h incubation with IL1-Alpha, and cytokines were measured using the ProcartaPlex 7-plex kit (Thermo Fisher Scientific, Cat# PPX-07-MXT2AW2, Lot# 333491-000/331205-000). Protein levels were determined using the Luminex FlexMAP 3D Multiplexing Microplate reader (Thermo Fisher Scientific). After 1 h incubation with IL1-Alpha, RNA was isolated using an RNA extraction kit (Macherey-Nagel Inc., Cat# 740466.4).

Quantitative PCR

RNA samples were retrotranscribed to cDNA using LunaScript RT SuperMix Kit following the manufacturer's protocol (New England Biolabs, Cat# E3010) and analyzed by quantitative PCR using the individual specific Taqman primer/probe sets (Supplementary Data 1) with the Taqman Fast Advanced Master Mix (Thermo Fisher Scientific, Cat# 4444558).

Protein Immunodetection

Whole-cell lysates (WCEs) were prepared through lysing cell pellets for 3 min in 1X protein sample loading buffer (LICORbio, Cat# 928-40004) supplemented with 10 mM β-mercaptoethanol and Halt Protease Inhibitor Cocktail (ThermoFisher Scientific, Cat# 78429) then subjected to sonication on a PIXUL Multi-Sample Sonicator (Active Motif, Cat #53130) according to the manufacturer's recommended settings. WCEs were clarified and run on a Jess Automated Western System (bio-technique/protein simple, Cat # 004-650) using the 12-230 kDa Separation Module (bio-technique/protein simple, Cat # SM-W001) according to manufacturer's recommended settings and utilizing an HA antibody (1:20 dilution, Cell Signaling Technology, Cat # CST2367S) and a CTCF loading control antibody (1:200 dilution, Cell Signaling Technology, Cat # CST3418S).

Neutrophil migration assay

IMR-90 cells were cultured and plated in EMEM (ATCC, Cat# 30-2003) at 100k cells/well in 6 well plates. Complete media was made with 10% FBS (VWR, Cat# 97068-085). IMR-90 cells were transfected by adding CXCL-EC to the media at a final concentration range of 1 µg/mL to 0.0008 µg/mL of mRNA formulated in SSOP lipid mix. Cells were incubated for 24 h with media containing LNPs. After 24 h, IL1-alpha (Life Technologies, Cat# PCH0015) was added at 10 ng/mL final concentration and incubated for 32 h. After incubation with IL1-alpha, the cell supernatant was collected used to conduct a neutrophil migration assay using IL1-alpha treated supernatant as a control to which the test groups were compared to a lower chamber, and neutrophils from six different human plasma donors were added separately to an upper chamber. After 1 h, the number of neutrophils were quantified at the lower chamber to assess neutrophil migration. Decreases in CXCL1-8 cytokine in the supernatant should decrease the migration of the neutrophils from the upper to the lower chamber.

CRISPR engineering K-562 MYC/d2GFP cell line

K-562 cells were modified to co-express d2GFP along with MYC as previously described¹⁸. Briefly, previously published MYC homology arms surrounding the P2A-d2GFP cassette were purchased from Azenta and cloned into the pUC-GW-Amp vector. An sgRNA was ordered from IDT to target the MYC 3' UTR (mC*mU*mU*rGrUrGrCrGrUrArArGrGrArArArGrUrArGrUrUrUrArGrArGrCrUrArGrArArUrArGrCrArArGrUrUrArArArUrArArGrGrCrUrArGrUrCrGrUrArUrCrArArCrUrUrGrArArArGrUrGrGrCrArCrGrArGrUrCrGrUrGrCmU*mU*mU*rU). RNPs were formed by combining equimolar ratios of sgRNA and recombinant spHiFi Cas9 Nuclease v3 (IDT, Cat# 1081060) protein and incubating at room temperature for 20 min. 1 million K-562 cells were electroporated with 2 µg of HDR plasmid and 250 pmol RNP using a Nucleofector 4D (Lonza) and the SF reagent kit (Lonza, Cat# V4XC-2032) according to the manufacturer's instructions.

Cells were allowed to recover and expand for 7 days, and then GFP+ cells were sorted 5 cells/well into a 96-well plate by fluorescence-activated cell sorting (FACS, with a gating strategy provided in Supplementary Fig 6). Clone pools were allowed to expand for an additional 7 days and then were genotyped by lysate PCR for the d2GFP insert using primers directed to MYC exon 3 and the 3'-UTR (Supplementary Data 1). Homozygously edited clonal pools containing only the modified allele, which were not heterozygous for the wild-type and modified allele, were identified via gel electrophoresis and selected for an additional PCR screen to verify proper integration using primers directed to MYC intron 2 and d2GFP (Supplementary Data 1). Clone pools were subjected to a limiting dilution in a 96-well plate to identify single-cell clones that were PCR genotyped with both assays to ensure a pure population.

Chromatin immunoprecipitation followed by high-throughput sequencing (ChIP-Seq)

ChIP-seq was performed via high-throughput ChIPmentation as previously described³⁷. Briefly, 500,000 cells were cross-linked in 1% formaldehyde for 15 min and quenched with 275 mM glycine prior to flash freezing and storage at -80°C . p65 ChIP was performed using double-crosslinking with 1.5 mM EGS incubated for 30 mins and spun down for 5 mins at $5000 \times g$. The supernatant was discarded, and the pellet was resuspended in 1% formaldehyde. Samples were then incubated for 10 mins, spun down for 5 mins at $5000 \times g$, and the pellet was flash frozen. Antibodies for HA (3 μg , EpiCypher, Cat# 13-2010), H3K9me3 (1 μg , Diagenode, Cat# C15410193), p65 (3 μl , Cell Signaling, Cat# 8242), or H3K27Ac (3 μg , Abcam, Cat# Ab4729) were loaded onto Protein G Dynabeads (1009D, Life Technologies) in PBS and 0.5% BSA for 4 h, rotating at 4°C . Fixed cells were thawed in Cell Lysis Buffer (50 mM Tris HCl, 10 mM EDTA, 0.5% SDS) and HALT Protease Inhibitor (Thermo Fisher Scientific, Cat# 87786) and then processed via multi-modal shearing using a probe-based sonicator (QSonica) followed by the PIXUL acoustic Sonicator (Active Motif). An input fraction was reserved, and cell lysates were transferred onto pre-loaded antibody-bead conjugates for immunoprecipitation overnight, rotating at 4°C .

Following immunoprecipitation, beads were washed prior to on-bead tagmentation of chromatin using Tagment DNA Enzyme 1 (Illumina, Cat# 20034197). Both immunoprecipitate and input fractions were tagmented for 10 min at 37°C with shaking. Samples were washed and PCR amplified for 12 cycles using HiFi MasterMix (New England Biolabs, Cat# M0541) and combinatorial i5/i7 primers derived from Mezger A, et al.³⁸. The PCR protocol included an initial 5 min 72°C incubation for gap-filling and a 5-minute incubation at 95°C , sufficient for cross-linking reversal. Final libraries were purified using SPRI beads (1X SPRISelect, Beckman Coulter, Cat# B23318), pooled at equimolar ratios, and sequenced on a NextSeq 2000 Sequencing System (Illumina) using a 2 \times 50 PE strategy. Each library was sequenced, targeting a depth of 30 M raw reads/fragments.

Illumina sequencing data in FASTQ format was collected and QCed using FASTQC³⁹ to ensure the NGS quality of reads before starting the ChIP-Seq analysis pipeline. Illumina sequencing adapters were trimmed using Trimmomatic (v0.6.7) to eliminate technical sources of ChIP-Seq bias. Trimmomatic reads were aligned to human genome hg19 using Bowtie2⁴⁰ to create the initial mapped BAM files⁴¹. Mapped reads in the BAM files were sorted and filtered to remove duplicate reads in the generated duplicated BAM files using Picard⁴² (v3.1). MACS2⁴³ (v2.2.7.1) was applied on filtered BAM files of individual ChIP samples to call ChIP peaks using FDR < 0.05 against input control.

3' DGE RNA-Seq

3' Digital Gene Expression (DGE) RNA-seq was performed using the Lexogen QuantSeq 3' mRNA-seq V2 kit (Lexogen Cat# 191.24) according to the manufacturer's instructions. Briefly, 250 ng of total

RNA was input into first-strand synthesis using oligo(dT) priming and subsequent RNA removal. Second-strand synthesis was performed using random priming followed by cDNA purification via SPRI-beads. Library amplification was performed using 12 nt UDIs over 17 PCR cycles and purified via SPRI-beads. Libraries were sequenced on a NextSeq 2000 using a 1 \times 100bp strategy.

Data was processed in accordance with the manufacturer's guidelines (QuantSeq 3' mRNA-Seq Integrated Data Analysis Pipelines on Bluebee® Genomics Platform 015UG108V0201). Briefly, UMItools (v1.1.4) was used to extract UMI barcodes and adapters were trimmed using TrimGalore (v0.6.10) and aligned to the mm10 reference genome using STAR (v2.7.11b). The deduplicated bam files are used as the inputs to HTSeq (v2.0.5) for quantification. Samples with less than 10 million reads passing QCs were filtered. Raw gene-level count data were imported using tximport, and differential expression was calculated using DESeq2 (v1.40.2) with the ~timepoint + treatment for the experiment-wide analysis.

Whole Genome Methylation Sequencing

Whole genome methylation sequencing libraries were prepared using the NEB Enzymatic Methyl-Seq Kit (NEB Cat #E7120L) according to the manufacturer's instructions. Briefly, gDNA was acoustically sheared using the PIXUL (Active Motif) to achieve ~300 bp fragments using the suggested protocol: Pulse 50 N/PRF 1 kHz/Burst 20 Hz/Time 36 min. 200 ng of sheared gDNA was end repaired and ligated with EM-seq adapters. Following SPRI bead purification, adapter-ligated DNA was enzymatically converted. Purified, converted DNA was dual-indexed and amplified by PCR using Q5U polymerase for 4 cycles. Final libraries were size-selected using a 0.85X SPRISelect bead purification, pooled at equimolar ratios, and sequenced on a NextSeq2000 using a 2 \times 150bp strategy. Bismark (v0.24.0) was used to align raw sequencing reads to a converted hg19 genome and estimate the CpG methylation level. DMRSeq (v1.26) was used to identify differentially methylated regions (DMR) between the treatment groups from the raw methylation estimate. The 'adjustCovariate' parameter was set to control time points.

Amplicon methylation sequencing

Genomic DNA was normalized to 200 ng in 100 μl low Tris-EDTA (TE) buffer and sheared briefly using the PIXUL (Active Motif) to obtain fragments less than 15 kb in size: 5 Pulse/1 kHz PRF/3 min/20 Hz Burst. Fragmented DNA was purified using 1X SPRI-Select (Beckman-Coulter) and subjected to EM-conversion using the EM-seq Conversion Kit (New England Biolabs, Cat# E7125) according to the manufacturer's instructions. Purified, converted DNA was PCR amplified for 40 cycles at the locus of interest using Q5U MasterMix (New England Biolabs, Cat# M0597) according to the manufacturer's instructions using the primers in Supplementary Data 1 (500 nM each in 20 μl reactions).

Following SPRI bead purification (1.8X SPRISelect, Beckman Coulter), the amplicon was transposase-labeled with Illumina sequencing adapters using Tagment DNA Enzyme 1 (20034197, Illumina). Tagmentation was performed using 0.1 μl enzyme per 10 μl reaction containing approximately 30 ng of the amplicon for 5 min at 37°C , and the reaction was stopped with 0.04% SDS. Libraries were dual-indexed (combinatorial) via PCR using KAPA HiFi ReadyStart MasterMix (KK2602, Roche Sequencing Store) and i5/i7 primers derived from Mezger A, et al.³⁸. PCR reactions occurred in 40 μl volumes with 100 nM of each primer for 13 cycles.

Final libraries were purified using SPRI beads (1X SPRISelect, Beckman Coulter), pooled at equimolar ratios, and sequenced on a MiSeq System (Illumina) using a v2 Nano 2 \times 150bp reagent kit (MS-103-1001, Illumina). The sequencing reads were trimmed, and Bismark⁴⁴ was used for read alignment and quantification. The mean methylation values were estimated based on the methylated ratio of individual CpGs.

Flow cytometry and sorting of K-562 MYC/d2GFP cells

K-562 (wild-type) and K-562 MYC/d2GFP cells were grown in complete media (RPMI-1640; 11875, Gibco + 10% FBS; S11550, Atlanta Biologicals + 1% Pen/Strep; 15140, Gibco) and 3 million cells were seeded into T75 flasks. Cells were treated with MYC-EC or JQ1 (4499; Torcis) at the specified concentrations by direct addition to the media; separate flasks were used to culture single-color controls (untreated K-562 MYC/dsGFP and MYC-EC-treated K-562 wild-type). MYC-EC-treated and JQ1-treated cells were harvested after 44 h and 16 h, respectively, by centrifugation at $400 \times g$ for 5 min and resuspended in PBS.

In dosage, titration experiments, cell suspensions were directly plated (200 μ l/well) in a round bottom 96-well plate (3879; Costar) and analyzed on an Aurora flow cytometer (Cytek). 100,000 events were collected from three independent experiments. Cells were gated to identify live, single-cells based on FSC/SCC, and GFP populations were determined by comparing histograms of untreated controls with the MYC-EC 4 μ g/ml condition.

In sorting experiments, cell suspensions were filtered through a cell strainer (352235; Falcon) prior to sorting on an MA900 cell sorter (Sony Biotechnology). A 130 μ m chip (LE-C3213; Sony Biotechnology) and automated setup beads (LE-B3001; Sony Biotechnology) were used to establish optimal instrument settings for gating and sorting. Cells were gated to identify live, single-cells based on FSC/BSC, and GFP-/tdTomato + or GFP + /tdTomato- cells were sorted and collected off a biaxial plot (eGFP vs. tdTomato). An unsorted population was reserved prior to loading onto the sorter. The genomic DNA of collected cells was extracted using the DNeasy Blood & Tissue Kit (69516; Qiagen), and the entire eluate was used as input for amplicon methylation sequencing. FlowJo 10.8.1 (BD Biosciences) was used for cytometric analysis.

Laboratory animals used in this manuscript

C57BL/6 normal (Jackson Labs inbred B6; strain #000664) mice (*Mus musculus*) were used in the *Pcsk9* and *Cxcl* studies at the ages described in each experiment. Transgenic Ai14 (B6.Cg-Gt(ROSA)^{26Sortm14(CAG-tdTomato)Hze/J}, Jackson Labs strain #007914) mice (*Mus musculus*), aged 6–8 weeks old, were used in the LNP biodistribution study. Animals were housed in groups of 5 animals per cage, with AlphaDri[®], wood shavings, or corn cob as bedding, which was changed once per week at minimum. Animals were acclimatized prior to the commencement of each study, during which the animals were observed to identify any that were present in poor condition. The studies were performed at facilities provided by Pharma Models, MLM Medical Labs, or Biomere Biomedical Research Models, Inc., where animal rooms were kept at a temperature of $70 \pm 5^\circ\text{F}$ and $50\% \pm 20\%$ relative humidity with 10–15 air changes per hour. The room provided cycles of 12 h light followed by 12 h dark with no twilight. Each facility retained records of temperature and relative humidity. Animals were fed with Envigo 2920X or equivalent commercial sterile rodent chow. Sterile water was provided ad libitum.

In vivo Pcsk9 pilot study

Forty female C57BL/6 mice (approximately 14 weeks old) were subdivided into 4 groups (10 mice each) and were treated via tail vein injection with the indicated dose of the EC or PBS control. At 7 days post-administration, serum and liver punches were isolated. Liver punches were homogenized, and RNA was isolated. RNA was then converted to cDNA. cDNA was analyzed by multiplexed qPCR using TaqMan probes specific to *Hprt1* (housekeeper) and *Pcsk9*. Relative *Pcsk9* mRNA expression was determined through the comparative delta-delta Ct method. Serum Pcsk9 levels were detected using the Mouse Pcsk9 ELISA Kit (ab215538, Abcam). This study was performed at Pharma Models (Marlborough, MA).

In vivo Pcsk9 long-term study

140 female C57BL/6 mice (approximately 6 to 7 weeks old) were subdivided into 2 groups (70 mice each) and were treated via tail vein injection with 3 mg/kg of the EC or PBS control. Serum samples were collected every two weeks and analyzed for Pcsk9 content. Ten mice from each group were sacrificed starting at 14 days post-injection, then monthly through six months. Liver punches were isolated and analyzed for *Pcsk9* promoter methylation by amplicon methylation sequencing. This study was performed at Pharma Models (Marlborough, MA).

Cxcl1-8 In vivo read-outs

Female C57BL/6 mice (approximately 14-weeks old) received a 1 mg/kg iv administration of the MM-Cxcl-EC₁/MM-Cxcl-EC₂ combination or GFP control in an LNP formulation 8 h prior to the LPS challenge, 10 mice per arm. 50 μ L of LPS was administered by oropharyngeal aspiration into each animal at 0 h. Mice were monitored and samples of BALF and peripheral blood were collected at 24 h after LPS challenge for flow cytometric analysis. Using the antibodies Ly6G-FITC (dil, Biolegend, Cat# 127605), CD45-BV605 (dil, Biolegend, Cat# 103155), B220-PE-Cy7 (dil, Tonbo, Cat# 60-0452), SiglecF-BV421 (dil, Biolegend, Cat# 155509), CD3-PE (dil, Biolegend, Cat# 100205), CD11b-BV785 (dil, Biolegend, Cat# 101243), and CD11c-PerCP/Cy5.5 (dil, Biolegend, Cat# 117327) and the gating strategy illustrated in Supplementary Fig 7, neutrophils were identified as CD45 +, Siglec F-, CD11b +, CD11c-, Ly6G +, T cells were identified as CD45 +, Siglec F-, CD11c-, CD3 +, and B cells were identified as CD45 +, Siglec F-, CD11c-, B220 +. Body weights were measured on the day of treatment and 1-day pre and post-treatment for ten animals per group. For Immunohistochemistry (IHC), one animal from each group was used to examine morphologic pathology of the lung. Lungs were inflated and fixed with formalin and H&E staining for inflammation and cell infiltration assessment. This study was executed at MLM Medical Labs, Inc. (Minneapolis, MN).

LNP Biodistribution study

Three female Ai14 mice, 6–8 weeks-old, were dosed intravenously with 3 mg/kg of Cre mRNA (TriLink, Cat# L-7211) loaded into DOTAP LNPs for overall assessment of LNP biodistribution, with a qualitative assessment of sections based on cell morphology. The liver, lungs, and spleen were dissected 48 h post-LNP treatment for quantification of tdTomato reporter protein activity. The organs were imaged at 554/581 Ex/Em (nm) in a Perkin Elmer IVIS Spectrum S3 Imaging System. tdTomato activity was expressed as radiance (photons/sec/cm²/steradian). This study was performed at Biomere Biomedical Research Models, Inc. (Worcester, MA).

The dissected organs were fixed for 24 h in 10% Neutral Buffered Formalin. Tissues were further dehydrated in Ethanol and embedded into paraffin blocks for immunohistochemistry (IHC) analysis. Rabbit anti-RFP antibody (1:300 dilution, Novus Biologicals, Cat# NBPI-72732C) and anti-rabbit HRP/DAB micro-polymer antibody (Abcam, Cat# Ab236469) were used as primary and secondary antibodies, respectively. A peroxidase-based detection kit (ImmPACT[®], Cat# SK-4103) was used to develop the color of tdTomato reporter protein in the tissue.

Statistics and reproducibility

For each in vivo study, the specific numbers and strains of mice used are listed in the method and figure legends. Mice were randomized into control and treatment groups prior to treatment. No statistical method was used to predetermine the sample size. The numbers of animals used were sufficient to generate sufficient statistical assessment (using one-way or two-way ANOVA) at the end of treatment periods. For each in vivo study, the study director at the animal facility were not blinded to the treatment modality. Results are presented

from one independent study each. For the in vivo studies, ROUT outlier detection methods were applied.

All in vitro experiments were repeated in greater than or equal to two biological replicates with greater than or equal to two technical replicates included. Specific replicates are listed in figure legends. In vitro experiments were not randomized. For in vitro experiments, the investigators were not blinded to allocation during experiments and outcome assessment. Statistics for figures were calculated using GraphPad Prism (version 10.4.1) algorithms and were one- or two-way ANOVA tests or *t* tests as indicated in individual figure legends. All *t* tests were unpaired, two-tailed unless otherwise indicated in the figure legend. Multiple-testing was performed (BH-FDR) when multiple *t* tests were examined and verified to be $q < 0.05$. Error bars represent means \pm standard deviation as calculated by GraphPad Prism. No data were excluded from the analyses.

Statistical significance and effect sizes for differentially methylated regions (Table 1) were calculated using the R (v4.3.1) package DMRSeq⁴⁵ (v1.26) where beta represents the coefficient value for treatment effect. DMRs were filtered based on an adjusted *p*-value threshold of 0.05 calculated using the Benjamini-Hochberg method (BH-FDR).

Statistical significance and Log2-fold-change (log2FC) of normalized counts for differentially expressed genes were calculated using the R package DESeq2⁴⁶ (v1.40.2) using the design “~ timepoint + treatment” for the experiment-wide analysis and a BH-FDR adjusted *p*-value of < 0.05 considered significant.

Reporting summary

Further information on research design is available in the Nature Portfolio Reporting Summary linked to this article.

Data availability

All source data supporting the findings of this study are available within the paper and its Supplementary Information and Source Data file. Individual data points are shown when possible and/or included in the Source Data file. The raw human ChIP-seq data generated in this study have been deposited in the NIH Sequence Read Archive (SRA) under bioproject [PRJNA1047162](https://www.ncbi.nlm.nih.gov/bioproject/PRJNA1047162). The raw longitudinal mouse EM-seq data for *Pcsk9* and paired RNA-seq and WGM-seq data were deposited under SRA bioproject [PRJNA1050224](https://www.ncbi.nlm.nih.gov/bioproject/PRJNA1050224). All data are publicly available. No new algorithms were developed for this study. Source data are provided in this paper.

References

- Visscher, P. M. et al. 10 Years of GWAS discovery: Biology, function, and translation. *Am. J. Hum. Genet.* **101**, 5–22 (2017).
- Maurano, M. T. et al. Systematic localization of common disease-associated variation in regulatory DNA. *Science* **337**, 1190–1195 (2012).
- Shilatifard, A. Chromatin modifications by methylation and ubiquitination: implications in the regulation of gene expression. *Annu. Rev. Biochem.* **75**, 243–269 (2006).
- Downen, J. M. et al. Control of cell identity genes occurs in insulated neighborhoods in mammalian chromosomes. *Cell* **159**, 374–387 (2014).
- Feehley, T., O'Donnell, C. W., Mendlein, J., Karande, M. & McCauley, T. Drugging the epigenome in the age of precision medicine. *Clin Epigenetics* **15**, 6 (2023).
- Mancarella, D. & Plass, C. Epigenetic signatures in cancer: proper controls, current challenges and the potential for clinical translation. *Genome Med.* **13**, 23 (2021).
- Watts, J. K. & Corey, D. R. Silencing disease genes in the laboratory and the clinic. *J. Pathol.* **226**, 365–379 (2012).
- Naso, M. F., Tomkowicz, B., Perry, W. L. 3rd & Strohl, W. R. Adeno-associated virus (AAV) as a vector for gene therapy. *BioDrugs* **31**, 317–334 (2017).
- Senapedis, W. et al. Targeted transcriptional downregulation of MYC using epigenomic controllers demonstrates antitumor activity in hepatocellular carcinoma models. *Nat. Commun.* **15**, 7875 (2024).
- Ha, H., Debnath, B. & Neamati, N. Role of the CXCL8-CXCR1/2 Axis in cancer and inflammatory diseases. *Theranostics* **7**, 1543–1588 (2017).
- Williams, A. E. et al. Evidence for chemokine synergy during neutrophil migration in ARDS. *Thorax* **72**, 66–73 (2017).
- Lukaszewicz-Zajac, M., Paczek, S., Mroczko, P. & Kulczynska-Przybik, A. The significance of CXCL1 and CXCL8 as well as their specific receptors in colorectal cancer. *Cancer Manag. Res.* **12**, 8435–8443 (2020).
- Amabile, A. et al. Inheritable silencing of endogenous genes by hit-and-run targeted epigenetic editing. *Cell* **167**, 219–232 (2016).
- Cappelluti, M. A. et al. Durable and efficient gene silencing in vivo by hit-and-run epigenome editing. *Nature* **627**, 416–423 (2024).
- Cermak, T. et al. Efficient design and assembly of custom TALEN and other TAL effector-based constructs for DNA targeting. *Nucleic Acids Res.* **39**, e82 (2011).
- Xia, X.-d et al. Regulation of PCSK9 expression and function: Mechanisms and therapeutic implications. *Front. Cardiovasc. Med.* **8**, 764038 (2021).
- Li, X. et al. Generation of destabilized green fluorescent protein as a transcription reporter. *J. Biol. Chem.* **273**, 34970–34975 (1998).
- Steinberger, J. et al. Tracing MYC expression for small molecule discovery. *Cell Chem. Biol.* **26**, 699–710 e696 (2019).
- Jiang, G., Deng, W., Liu, Y. & Wang, C. General mechanism of JQ1 in inhibiting various types of cancer. *Mol. Med. Rep.* **21**, 1021–1034 (2020).
- Filippakopoulos, P. et al. Selective inhibition of BET bromodomains. *Nature* **468**, 1067–1073 (2010).
- Jurida, L. et al. The activation of IL-1-induced enhancers depends on TAK1 kinase activity and NF- κ B p65. *Cell Rep.* **10**, 726–739 (2015).
- Modi, W. S. & Yoshimura, T. Isolation of novel GRO genes and a phylogenetic analysis of the CXC chemokine subfamily in mammals. *Mol. Biol. Evol.* **16**, 180–193 (1999).
- Fan, X. et al. Murine CXCR1 is a functional receptor for GCP-2/CXCL6 and interleukin-8/CXCL8. *J. Biol. Chem.* **282**, 11658–11666 (2007).
- Asfaha, S. et al. Mice that express human interleukin-8 have increased mobilization of immature myeloid cells, which exacerbates inflammation and accelerates colon carcinogenesis. *Gastroenterology* **144**, 155–166 (2013).
- Gao, H., Ying, S. & Dai, Y. Pathological roles of neutrophil-mediated inflammation in Asthma and its potential for therapy as a target. *J. Immunol. Res.* **2017**, 3743048 (2017).
- Walters, E. H., Ward, C. & Li, X. Bronchoalveolar lavage in asthma research. *Respirology* **1**, 233–245 (1996).
- Madisen, L. et al. A robust and high-throughput Cre reporting and characterization system for the whole mouse brain. *Nat. Neurosci.* **13**, 133–140 (2010).
- Tecchio, C., Micheletti, A. & Cassatella, M. A. Neutrophil-derived cytokines: facts beyond expression. *Front. Immunol.* **5**, 508 (2014).
- Mancino, A. & Lawrence, T. Nuclear factor- κ B and tumor-associated macrophages. *Clin. Cancer Res.* **16**, 784–789 (2010).
- Buocikova, V. et al. Epigenetics in breast cancer therapy-new strategies and future nanomedicine perspectives. *Cancers* **12**, <https://doi.org/10.3390/cancers12123622> (2020).
- Nuñez, J. K. et al. Genome-wide programmable transcriptional memory by CRISPR-based epigenome editing. *Cell* **184**, 2503–2519 (2021).
- Hou, X., Zaks, T., Langer, R. & Dong, Y. Lipid nanoparticles for mRNA delivery. *Nat. Rev. Mater.* **6**, 1078–1094 (2021).
- Cullis, P. R. & Felgner, P. L. The 60-year evolution of lipid nanoparticles for nucleic acid delivery. *Nat. Rev. Drug Discov.* **23**, 709–722 (2024).

34. Sun, Y. et al. In vivo editing of lung stem cells for durable gene correction in mice. *Science* **384**, 1196–1202 (2024).
35. Polack, F. P. et al. Safety and efficacy of the BNT162b2 mRNA covid-19 vaccine. *N. Engl. J. Med.* **383**, 2603–2615 (2020).
36. Baden, L. R. et al. Efficacy and safety of the mRNA-1273 SARS-CoV-2 vaccine. *N. Engl. J. Med.* **384**, 403–416 (2021).
37. Gustafsson, C., De Paepe, A., Schmidl, C. & Mansson, R. High-throughput ChIPmentation: freely scalable, single day ChIPseq data generation from very low cell-numbers. *BMC Genomics* **20**, 59 (2019).
38. Mezger, A. et al. High-throughput chromatin accessibility profiling at single-cell resolution. *Nat. Commun.* **9**, 3647 (2018).
39. Babraham Bioinformatics. FastQC. (2023).
40. Bowtie. Bowtie 2. (2023).
41. Samtools. Sequence Alignment/Map Format Specification. The SAM/BAM Format Specification Working Group. (2022).
42. GATK. MarkDuplicates (Picard). (2022).
43. Github. MACS2 2.2.8. MACS: Model-based Analysis for ChIP-Seq. (2023).
44. Babraham Bioinformatics. Bismark. (2023).
45. Korthauer, K., Chakraborty, S., Benjamini, Y. & Irizarry, R. A. Detection and accurate false discovery rate control of differentially methylated regions from whole genome bisulfite sequencing. *Biostatistics* **20**, 367–383 (2019).
46. Love, M. I., Huber, W. & Anders, S. Moderated estimation of fold change and dispersion for RNA-seq data with DESeq2. *Genome Biol.* **15**, 550 (2014).

Acknowledgements

This work was supported by internal funding from Omega Therapeutics. We would like to thank Dana Barberio, MS of Edge Bioscience Communications, for her contribution to writing and editing the manuscript, and Anne Tsimboukis of Refine Design for contributions to figure graphics.

Author contributions

C.W.O., J.D.F., H.B., J.C., J.V.N. and T.G.M. contributed to the conceptualization of platform methodology and all studies presented in this article, data review and interpretation, and writing. C.W.O., J.D.F., H.B., J.C., and C.M.-S. contributed to the design of epigenetic controllers. C.W.O., J.D.F., H.B., J.C., L.B., J.S., C.M.-S., A.K., S.M., M.G., G.C.C., and P.D. contributed to coordination and execution of in vitro results, data analysis, review, and interpretation. J.D.F., C.M.-S., M.G., P.D., C.R.W., P.R., D.F.G.C., M.I.G., and J.V.N. contributed to the coordination and

execution of in vivo studies and results. S.S. and Y.E.W. contributed to high-dimensional data processing, analysis, review, and interpretation.

Competing interests

All authors were employees of Omega Therapeutics when the work was conducted. All authors were or currently are shareholders of Omega Therapeutics stock and/or options. T.G.M. is the former Chief Scientific Officer of Omega Therapeutics.

Additional information

Supplementary information The online version contains supplementary material available at <https://doi.org/10.1038/s41467-025-57920-5>.

Correspondence and requests for materials should be addressed to Charles W. O'Donnell.

Peer review information *Nature Communications* thanks Lior Zangi and the other anonymous reviewer(s) for their contribution to the peer review of this work. A peer review file is available.

Reprints and permissions information is available at <http://www.nature.com/reprints>

Publisher's note Springer Nature remains neutral with regard to jurisdictional claims in published maps and institutional affiliations.

Open Access This article is licensed under a Creative Commons Attribution-NonCommercial-NoDerivatives 4.0 International License, which permits any non-commercial use, sharing, distribution and reproduction in any medium or format, as long as you give appropriate credit to the original author(s) and the source, provide a link to the Creative Commons licence, and indicate if you modified the licensed material. You do not have permission under this licence to share adapted material derived from this article or parts of it. The images or other third party material in this article are included in the article's Creative Commons licence, unless indicated otherwise in a credit line to the material. If material is not included in the article's Creative Commons licence and your intended use is not permitted by statutory regulation or exceeds the permitted use, you will need to obtain permission directly from the copyright holder. To view a copy of this licence, visit <http://creativecommons.org/licenses/by-nc-nd/4.0/>.

© The Author(s) 2025